

Electrophoretic Properties of Highly Charged Colloids: A Hybrid MD/LB Simulation Study

Apratim Chatterji^{1,2}, Jürgen Horbach¹

¹*Institut für Physik, Johannes-Gutenberg-Universität, Staudinger Weg 7, D-55099 Mainz, Germany*

²*Department of Physics, University of Toronto, 60 St. George Street, Toronto M5S-1A7, Canada*

Using computer simulations, the electrophoretic motion of a positively charged colloid (macroion) in an electrolyte solution is studied in the framework of the primitive model. In this model, the electrolyte is considered as a system of negatively and positively charged microions (counterions and coions, respectively) that are immersed into a structureless medium. Hydrodynamic interactions are fully taken into account by applying a hybrid simulation scheme, where the charged ions (i.e. macroion and electrolyte), propagated via molecular dynamics (MD), are coupled to a Lattice Boltzmann (LB) fluid. In a recent electrophoretic experiment by Martin-Molina *et al.* [J. Phys. Chem. B **106**, 6881 (2002)], it was shown that, for multivalent salt ions, the mobility μ initially increases with charge density σ , reaches a maximum and then decreases with further increase of σ . The aim of the present work is to elucidate the behaviour of μ at high values of σ . Even for the case of monovalent microions, we find a decrease of μ with σ . A dynamic Stern layer is defined that includes all the counterions that move with the macroion while subject to an external electrical field. The number of counterions in the Stern layer, q_0 , is a crucial parameter for the behavior of μ at high values of σ . In this case, the mobility μ depends primarily on the ratio q_0/Q (with Q the valency of the macroion). The previous contention that the increase in the distortion of the electric double layer (EDL) with increasing σ leads to the lowering of μ does not hold for high σ . In fact, we show that the deformation of the EDL decreases with increase of σ . The role of hydrodynamic interactions is inferred from direct comparisons to Langevin simulations where the coupling to the LB fluid is switched off. Moreover, systems with divalent counterions are considered. In this case, at high values of σ the phenomenon of charge inversion is found.

PACS numbers: 75.60.Ej, 75.50.Lk

I. INTRODUCTION

The electrophoretic motion of charged macroions in an electric field \mathbf{E} is a longstanding issue in colloid science [1, 2, 3, 4, 5, 6, 7, 8, 9, 10, 11]. A complex interplay occurs between hydrodynamic, electrostatic, and thermal forces. A macroion of charge Q drags along an electric double layer (EDL) of small counterions with it and the number of charges “bound” in the EDL depends on the charge density, surface properties, ion concentration and liphophilicity of the macroion as well as the specific properties of counterions and salt ions [12]. Since it is difficult to experimentally probe and control these different parameters at microscopic length and time scales, the interpretation of experimental results often remains unclear. There is, e.g., no clear understanding of the variation of the mobility μ with the surface charge density σ of the macroion [13, 14, 15].

Most of the theoretical studies on electrokinetic phenomena consider the Coulomb interactions between macroions on the level of the linearized Poisson-Boltzmann equation [3, 6, 7]. This equation, valid for weakly charged macroions and low salt concentration, describes the formation of an EDL. It results in a screened Coulomb potential (Yukawa potential) as the effective interaction potential between the macroions. The central parameter of this potential is the Debye screening length $\lambda_D \equiv 1/\kappa$ (with κ the screening parameter) that measures the spatial extent of the EDL. When a charged

colloid moves in the presence of an electric field, the spherical EDL is distorted and it is coupled to the hydrodynamic flow of the solvent. In theoretical approaches [4, 13, 16, 17, 18], hydrodynamic effects are incorporated by coupling the Poisson equation for the electrostatics to the Navier-Stokes equations. In the resulting electrokinetic equations [5], so-called ζ potential is a central quantity. It is defined as the electrostatic potential $\psi(z_s)$ at a distance z_s from the colloidal surface where the fluid around the colloid is at rest with respect to the colloid motion. The imaginary surface at distance z_s from the colloidal surface is called surface of shear or slipping surface [4, 5, 17, 18]. Some of the counterions that are between the surface of the macroion and the surface of shear are often assumed to move along with the macroion and define the so-called *dynamic* Stern layer [5, 17].

The ζ potential can be related to the electrophoretic mobility $\mu = V_M/E$ (with V_M the steady-state macroion velocity). In the Helmholtz-Smoluchowski limit, i.e. for $\kappa R_M \rightarrow \infty$ (with R_M the radius of the macroion), the mobility of the macroion can be obtained from the ζ potential via $\mu = \epsilon \zeta(z_s)/\eta$ [2, 13, 18], where ϵ is the permittivity of the surrounding medium and η is the shear viscosity of the fluid. In the opposite Hückel-Onsager limit, $\lambda_D \gg R_M$, the mobility is given by $\mu = 2\epsilon \zeta(z_s)/3\eta$ [3]. The definition of the potential $\zeta(z_s)$ at the surface of shear is usually based on no-slip boundary conditions at the colloidal surface [18]. Since $\kappa R_M \rightarrow \infty$ implies a very small Debye length, the distance of the

surface of shear from the colloidal surface would be typically in the nanometer range. At such length scales the validity of no-slip boundary condition is not clear (although a hydrodynamic description might be still valid [19]). Calculations of μ which cover the entire range κR_M from the Helmholtz–Smoluchowski limit to the Hückel–Onsager limit have been done by Henry [3]. But these calculations, valid for low ζ , assumed that the counterion charge density is unaffected by the applied field.

O’Brien and White [7] did extensive numerical calculations to calculate μ versus ζ for different values of κR_M in the framework of electrokinetic equations. For $\kappa R_M > 3$, they obtained a pronounced maximum when plotting μ as a function of ζ . This behaviour is attributed to the competition between the driving force due to E and the retarding forces due to the distortion of the charge cloud constituting the EDL. The driving force increases linearly with ζ (which is proportional to Q), whereas the retarding force is proportional to ζ^2 . Thus for high values of ζ , μ decreases with ζ because then the retarding force dominates. Moreover, O’Brien and White found that for multivalent ions, the position of the maximum shifts to lower values of ζ . They argue that the distortion of the double layer is increased by multivalent counterions resulting in the increase of retardation forces against the motion of the colloid. Qualitatively similar results were also obtained by the non-linear solution by Oshina *et al.* [8] and by perturbation expansion in powers of ζ by Booth [9] and Overbeek [10]. There are also other models of more microscopic origin which look at charged systems, but these models focus mainly on the structure and dynamics of the dynamic Stern layer in planar geometry [17, 18] rather than on electrophoretic properties of charged spherical colloids. Moreover, some of these studies disregard hydrodynamic interactions [17] or consider only zero-temperature properties [20].

Electrophoresis experiments on colloidal suspensions [12, 13, 21, 22, 23, 24, 25, 26] allow to determine accurately the electrophoretic mobility μ as a function of different parameters such as κR_M , surface charge density of colloids, etc. However, it is difficult to disentangle hydrodynamic effects from those due to electrostatic interaction. Moreover, in order to fit experimental data to theoretical models, “renormalized charges” of the colloids have to be introduced [25].

In a recent experimental study by Martín–Molina *et al.* [13], a maximum was found in the electrophoretic mobility μ , plotted as a function of the macroion’s surface charge density σ (note that there is a linear relationship between σ and the ζ potential in the framework of the linearized Poisson–Boltzmann equation). The latter maximum occurs in the case of a 2:1 (counterion-charge:coion-charge) electrolyte. A similar result can be also found in the numerical paper by O’Brien and White [7] for a 2:1 electrolyte. However, the experiments were performed for systems of highly charged macroion’s. In this case, it is not clear whether the calculations by O’Brien and White yield a correct description, even on a qualitative

level. In this work, we aim at addressing this issue by using computer simulation techniques that may elucidate electrophoresis with highly charged particles on a microscopic level.

Molecular dynamics (MD) simulations of colloidal systems suffer from the large separation in length and time scales of solvent and colloidal particles. The problem of simulating millions of solvent particles to account for hydrodynamic effects can, however, be circumvented by using simulation techniques such as the Lattice Boltzmann (LB) [27] method or other Navier–Stokes equation solver (see, e.g. [28]) to model the solvent. In this work, we employ a hybrid LB/MD method [29, 30] to investigate the electrophoretic motion of a highly charged macroion in an electrolyte solution, thereby modeling macroion and electrolyte in the framework of the so-called primitive model (in a similar way as in Ref. [31]). Our aim in particular is to investigate those structural and dynamical aspects of the EDL which are out of scope of mesoscopic theories.

In the following, we are interested in the case of high values of σ , i.e. the regime beyond the aforementioned maximum in the $\mu - \sigma$ curve. In particular the counterion distribution around the macroion is measured to provide insight into the electrical retarding forces affecting the mobility. In order to disentangle hydrodynamic from electrostatic effects, the hydrodynamic medium (LB fluid) is also switched off, thus simulating the system via Langevin dynamics. Systems with monovalent and divalent salt ions are considered. In the latter case, the phenomenon of charge inversion is observed.

The rest of the paper is organized as follows: We describe the LB/MD method in Sec. II. In Sec. IIIA, we present the results for the monovalent electrolyte solution (microions) and in Sec. IIIB, we focus on the charge inversion phenomenon with divalent microions. Finally, conclusions are given in Sec. IV.

II. MODEL AND DETAILS OF THE SIMULATION

The electrophoretic motion of a macroion in an electrolyte solution is studied in the framework of the so-called primitive model. We consider a system of a macroion of charge $Q = Z_M e$ (mass $M = 60$ a.u.) and microions of charge $Z_{ct} = -1e$ (counterions) and $Z_{co} = 1e$ (coions), each of which are of mass 4 a.u.. The interaction potential between a particle of type α and a particle of type β ($\alpha, \beta = M, ct, co$) separated by a distance r from each other is given by

$$u_{\alpha\beta} = \frac{Z_\alpha Z_\beta e^2}{4\pi\epsilon r} + A_{\alpha\beta} \exp\{-B_{\alpha\beta}(r - \sigma_{\alpha\beta})\} \quad (1)$$

where e is the elementary charge and ϵ the dielectric constant. We choose the value $\epsilon = 80\epsilon_0$ (with ϵ_0 the vacuum dielectric constant) for water at room temperature. The parameters $\sigma_{\alpha\beta}$ denote the distance between

two ions at contact, $\sigma_{\alpha\beta} = R_\alpha + R_\beta$, where R_α is the radius of an ion of type α . In the following, we use values for R_M that vary from 10 \AA to 20 \AA . For the microions, we set $R_{ct} = R_{co} = 1 \text{ \AA}$. The exponential in Eq. (1) is an approximation to a hard sphere interaction for two ions at contact. For the parameters $A_{\alpha\beta}$ we choose $A_{MM} = 1.84 \text{ eV}$, $A_{M,ct} = A_{M,co} = 0.05565 \text{ eV}$, and $A_{ct,ct} = A_{ct,co} = A_{co,co} = 0.0051 \text{ eV}$. The parameters $B_{\alpha\beta}$ are all set to 4.0 \AA^{-1} . The long-ranged Coulomb part of the potential and the forces were computed by Ewald sums in which we chose $\alpha_E = 0.05$ for the constant and a cutoff wavenumber $k_c = 2\pi\sqrt{66}/L$ in the Fourier part [32, 33]. The linear dimension L of the simulation box is $L = 160 \text{ \AA}$, using periodic boundary conditions. All simulations were done at the temperature $T = 297 \text{ K}$.

Now, the crucial step is to model the solvent. To a first approximation, the effect of the solvent on colloidal particles (macroions) can be described by a Langevin equation where one assumes that on the typical time scale of the colloidal particles their collisions with solvent particles are due to Gaussian random forces $\mathbf{f}_{r,i}$. These forces lead to a systematic friction force $-\xi_0 \mathbf{V}_i(t)$ on the colloids, where ξ_0 is the friction coefficient and $\mathbf{V}_i(t)$ the velocity of particle i at time t . The resulting equations of motion are

$$M \frac{d^2 \mathbf{R}_i}{dt^2} = \mathbf{F}_{c,i} - \xi_0 \mathbf{V}_i(t) + \mathbf{f}_{r,i}, \quad (2)$$

where \mathbf{R}_i and $\mathbf{V}_i(t)$ denote respectively position and velocity of a colloidal particle i ($i = 1, \dots, N$ with N the total number of colloids) and $\mathbf{F}_{c,i}$ is the conservative force acting on the particle. The Cartesian components of the random forces, $f_{r,i}^\alpha$ ($\alpha = x, y, z$), are uncorrelated random numbers with zero mean, i.e.

$$\langle f_{r,i}^\alpha(\mathbf{R}_i, t) \rangle = 0 \quad (3)$$

$$\langle f_{r,i}^\alpha(\mathbf{R}_i, t) f_{r,i}^\beta(\mathbf{R}'_i, t') \rangle = A \delta_{\alpha\beta} \delta(\mathbf{R}_i - \mathbf{R}'_i) \delta(t - t') \quad (4)$$

The amplitude A is determined by the fluctuation-dissipation theorem, $A = 2k_B T \xi_0$. In our model, the microions are also Brownian particles and in thermal equilibrium with the solvent.

Equations (2)–(4) still do not provide a complete description of the dynamics in colloidal suspensions. In these equations the mass and momentum transport by the solvent is ignored that leads to the hydrodynamic interactions between the colloidal particles. However, hydrodynamic interactions can be incorporated rather easily into the Langevin description by replacing the absolute velocity $\mathbf{V}_i(t)$ of particle i in Eq. (2) by its velocity relative to the fluid velocity field $\mathbf{u}(\mathbf{R}_i, t)$ at the position of the particle \mathbf{R}_i . The “hydrodynamic force” on particle i is then given by

$$\mathbf{F}_{\text{hyd},i} = -\xi_0 [\mathbf{V}_i(t) - \mathbf{u}(\mathbf{R}_i, t)] + \mathbf{f}_{r,i} \quad (5)$$

In a simulation, the velocity field $\mathbf{u}(\mathbf{R}_i, t)$ can be calculated from any Navier–Stokes equation solver, whereby

thermal fluctuations have to be included in the framework of fluctuating hydrodynamics. In this work, we use a Lattice–Boltzmann (LB) [27, 34] scheme to compute $\mathbf{u}(\mathbf{R}_i, t)$. Since the LB method yields the velocity field \mathbf{u} on a lattice, an interpolation scheme has to be used to determine \mathbf{u} at the position of the particle \mathbf{R}_i . Very recently, Ahlrichs and Dünweg [35] have proposed a hybrid MD/LB scheme on the basis of the frictional coupling force, Eq. (5), to simulate polymers in solution.

Up to now, we have considered the colloidal particles as point particles. However, real colloids are extended objects with rotational degrees of freedom. The problem is to “implant” an extended object such as a sphere of radius R_H into a LB fluid. To this end, we follow Ladd’s method [34] and represent the sphere (or any other object) by uniformly distributed boundary points on its surface, where the surface is permeable for the LB fluid. We have recently proposed a sphere model with 66 boundary nodes of mass $M/66$ with M being the total mass of the colloidal particle [29]. This model for a spherical particle is also considered in the following. Each of the boundary points is coupled to the LB fluid by the force given by Eq. (5). The total force on the particle is determined by the sum over the forces on the boundary nodes (of course, according to Newton’s third law, these forces with opposite sign are given back to the LB fluid). From this total force the torque on the particle is calculated, and the total force and torque are then used to update the translational and rotational velocity of the particle, respectively. More details on our MD/LB scheme can be found elsewhere [29].

For the LB fluid a standard D3Q18 model was used, with which we solved the linearized Navier–Stokes equations (the details of the D3Q18 model can be found in review articles and the book by Succi [27, 34]). We consider an incompressible fluid in the creeping flow limit (zero Reynolds number) in our studies. The kinematic viscosity was set to $\nu = 0.0238a^2/\tau$ with a the lattice constant and τ the elementary time unit of the LB fluid. The density of the LB fluid was set to $\rho = 1.0m_0/a^3$ (m_0 : mass unit of the LB fluid). Thermal fluctuations were introduced via the addition of Gaussian random numbers to the stress tensor as proposed by Ladd [34]. The LB fluid is modelled on a cubic lattice with 40^3 lattice nodes, thus the lattice constant is $a = 4 \text{ \AA}$ (for the linear dimension $L = 160 \text{ \AA}$ of the simulation box). The counterions and coions are considered as point particles with respect to the interaction with the LB fluid. The 66 boundary nodes of the macroion are placed on a sphere of radius $R_H = 10 \text{ \AA}$. The effective hydrodynamic radius and the viscous retarding force on the macroion is thus determined by R_H . On the other hand, the variation of R_M from 10 \AA to 20 \AA (see next section) allows a change of the macroion’s surface charge σ without changing the hydrodynamic coupling of the particle to the LB fluid. For the friction constant ξ_0 in the coupling force, Eq. (5), a total value of $6.6m_0/\tau$ is assigned to the macroion which corresponds to $\xi_0 = 0.1m_0/\tau$ for each of the 66 bound-

Q [e]	N_{ct}	N_{co}	κ [\AA^{-1}]	κR_M
121	471	350	0.127	2.54
255	555	300	0.133	2.66
351	651	300	0.137	2.74
401	651	250	0.126	2.52
601	801	200	0.141	2.82
801	1001	200	0.154	3.08

TABLE I: Charge of the macroion Q , number of counterions N_{ct} , number of coions N_{co} , and the corresponding values of the screening parameter κ and the dimensionless quantity κR_M that were used in the simulations for $R_M = 20 \text{ \AA}$.

ary nodes. In a recent publication [29], we have shown that this value of ξ_0 corresponds to nearly stick boundary conditions. For the microions, a different value for the friction coefficient is used, denoted by ξ_{0b} in the following. Below we discuss the influence of ξ_{0b} on the electrophoretic mobility (see Fig. 7). Unless otherwise noted, the value $\xi_{0b} = 0.025m_0/\tau$ was chosen. With respect to the LB fluid, the microions are treated as point particles, but we remind the reader that their Coulomb radii are set to $R_{\text{ct}} = R_{\text{co}} = 1 \text{ \AA}$.

We have done MD/LB simulations of a single macroion of charge Q in an electric field E_x pointing in the positive x direction. The charge Q was varied from $121e$ to $801e$. The number of counterions and coions (N_{ct} and N_{co} , respectively) used for a given value of Q are listed in Table I. Also included in this list is the Debye screening parameter $\kappa = [4\pi\lambda_B(n_{\text{ct}} + n_{\text{co}})/L^3]^{1/2}$ which was roughly kept constant around 0.13 \AA^{-1} (the Bjerrum length $\lambda_B = e^2/(4\pi\epsilon_r\epsilon_0k_B T)$ is in our case equal to about 7 \AA). For comparison, we also carried out simulations with a ‘‘Langevin dynamics’’ (LD) where the coupling to the LB fluid was switched off, i.e. $\mathbf{u}(\mathbf{R}, t) = 0$. For the LB/MD and LD simulations, the equations of motion were integrated by a Heun algorithm with a time step of 1 fs . This very small time step is necessary because we consider explicitly counterions and coions as microscopic particles.

The simulations were done as follows: We first equilibrated the system for 25000 time steps without electric field and without coupling to the LB fluid. Then, the system was coupled to the LB fluid and the electric field was switched on, followed by simulation runs over 400000 time steps. After 100000 time steps, the steady state was reached and the positions and velocities of the ions were stored every 500 time steps to determine the averaged quantities such as the steady state velocity V_M of the macroion.

III. RESULTS

Now the simulation results are presented for the steady-state electrophoretic motion of a macroion in an

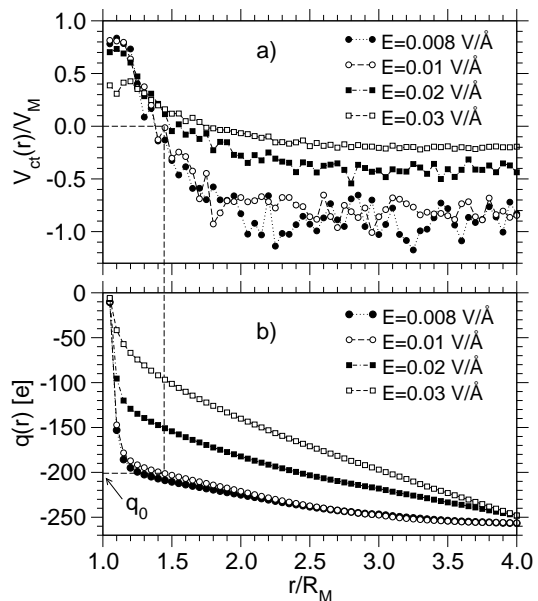


FIG. 1: a) $V_{\text{ct}}(r)/V_M$ as a function of r/R_M for different values of the electric field, as indicated. Data is shown for 1 macroion of charge $Q = 255e$, $N_{\text{ct}} = 555$ monovalent counterions and $N_{\text{co}} = 300$ monovalent coions. b) Cumulative counterion charge $q(r)$ for the same parameters as in a). q_0 is the cumulative counterion charge at which $V_{\text{ct}}(r)$ is zero. The determination of q_0 is indicated in the figure by the dashed lines for the example $E = 0.01 \text{ V/\AA}$.

electrolyte. Systems of highly charged macroions are considered, i.e. their surface charge densities vary between $\sigma = 0.02 e/\text{\AA}^2$ ($38 \mu\text{C}/\text{cm}^2$) and $\sigma = 0.3 e/\text{\AA}^2$ ($500 \mu\text{C}/\text{cm}^2$). The density of coions ($N_{\text{co}} = 300$) in our simulation box corresponds to a salt concentration of 0.012 mol/l .

A. Monovalent microions

In this section, we consider electrolyte solutions that consist of monovalent counter- and coions. For a microscopic understanding of electrophoresis, it is of particular interest to display the *dynamic* distribution of counterions in the vicinity of the macroion, i.e. in the EDL. This distribution is determined by an interplay between the electrostatic attraction and the hydrodynamic flow around the macroion. Some of the counterions in the EDL move along the same direction as the macroion, whereas, due to the electric field, other counterions in the EDL are accelerated in the opposite direction. We analyze the dynamic behavior of the counterions by their average velocity $V_{\text{ct}}(r)$ as a function of the radial distance r from the center of the macroion and the cumulative counterion charge $q(r)$ around the macroion.

First, we consider a system consisting of one macroion of charge $Q = 255e$, $N_{\text{ct}} = 555$ monovalent counterions and $N_{\text{co}} = 300$ monovalent coions. For this case, Fig. 1

displays $V_{\text{ct}}(r)/V_{\text{M}}$ (with V_{M} the steady state macroion velocity) and $q(r)$ for different choices of the electric field E . Within the statistical errors, the results essentially coincide for the two lowest values of the electric field, $E = 0.01 \text{ V/\AA}$ and $E = 0.008 \text{ V/\AA}$. The choice $E = 0.01 \text{ V/\AA}$ is used for all further results presented in this work, in particular for the estimates of the electrophoretic mobility, $\mu = V_{\text{M}}/E$. As shown previously [29], for $Q \geq 255e$ the linear response regime is essentially achieved for $E \leq 0.01 \text{ V/\AA}$.

From the behavior of $V_{\text{ct}}(r)/V_{\text{M}}$, different regions can be identified with respect to the distance from the center of the macroion. Close to the macroion's surface a layer with a thickness of about $0.25 R_{\text{M}}$ is formed where $V_{\text{ct}}/V_{\text{M}}$ is constant with a value around 0.8 for the two lowest values of E . In the following, this region is called the dynamic Stern layer, where, due to the electrostatic attraction by the macroion, counterions are essentially condensed onto the surface of the macroion. Beyond the Stern layer, the counterion velocity changes quickly its sign, thus indicating a motion in the direction opposite to that of the macroion. The point where the counterion velocity vanishes can be used as a measure of the extent of the Stern layer. As shown in Fig. 1, the cumulative counterion charge at this point, q_0 , is significantly smaller than the bare charge of the macroion (e.g. $q_0 \approx -200 e$ for $E = 0.01 \text{ V/\AA}$). Not until r is of the order of $3\text{--}4 R_{\text{M}}$, the counterion charge $q(r)$ is equal to the macroion's charge, thus completely neutralizing the latter. For high values of E , e.g. $E = 0.03 \text{ V/\AA}$, the counterions are stripped off the surface of the macroion, since the force due to the electric field dominates over the Coulomb attraction between macroion and counterions. This leads to a lower value of q_0 for high values of E and a less efficient shielding of the macroion compared to the case of low values of E . This in turn increases the velocity V_{M} of the macroion and thus explains the low values of $V_{\text{ct}}/V_{\text{M}}$ for large values of E at distances far from the colloidal surface.

One might expect, that the region between the Stern layer and the point where $q \approx Q$, is strongly affected by hydrodynamic flow features. That this is indeed the case can be inferred from a comparison to LD simulations where the coupling to the LB fluid is switched off (in the following, we refer to simulations with a coupling to LB as HD simulations).

In Fig. 2, $V_{\text{ct}}(r)/V_{\text{M}}$ from LD simulations is compared to the same quantity from HD simulations for the two macroion charges $Q = 255 e$ and $Q = 801 e$ (in the latter case the system contains $N_{\text{ct}} = 1001$ counterions and $N_{\text{co}} = 200$ coions). In the HD case, we see that for $Q = 801 e$, the ratio $V_{\text{ct}}(r)/V_{\text{M}}$ is very close to one in the Stern layer region. However, for $Q = 255 e$ the ratio is significantly smaller. The strong Coulomb attraction dominates the viscous drag and thermal fluctuations for high charges, such that layers of counterions nearest to the colloidal surface nearly stick to the surface. But for lower macroion charges, one starts to see deviations from the assumption that the *dynamic* Stern layer consists of

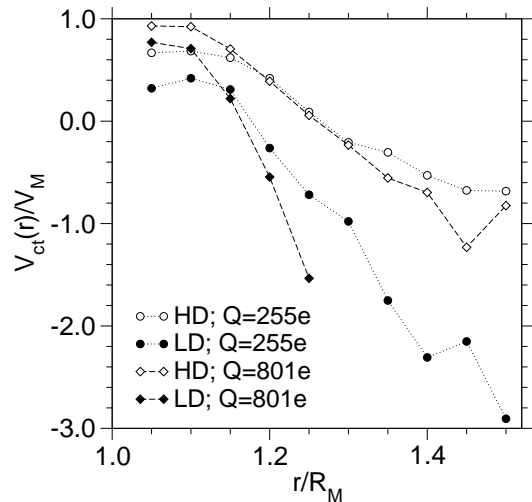


FIG. 2: $V_{\text{ct}}(r)/V_{\text{M}}$ as a function of r/R_{M} for two different values of the bare charge Q , as indicated. For the HD case, the data from Fig. 1 for $Q = 255 e$ and $E = 0.01 \text{ V/\AA}$ are plotted (open circles). The closed circles are the corresponding results from LD simulations. Also shown are results for $Q = 801$ (open and closed diamonds for HD and LD, respectively). In this case, the system contains $N_{\text{ct}} = 1001$ counterions and $N_{\text{co}} = 200$ coions.

immobile counterions [2, 18]. Moreover, the Stern layer is extended, and it is not restricted to one layer of microions closest to the macroion surface as observed in [18]. This is due to the much higher values of the surface charge density σ used in our study.

As indicated by Fig. 2, in the LD case the motion of the counterions is less correlated to that of the macroion than in the HD case. The value of $V_{\text{ct}}(r)/V_{\text{M}}$ is smaller in the Stern layer region than in the corresponding HD data. Moreover, the counterions reverse their velocity at about $0.15 R_{\text{M}}$ away from the macroion surface, followed by a more rapid decrease of $V_{\text{ct}}(r)/V_{\text{M}}$ than in HD. From data presented below (in Fig. 4), we will see that the number of counterions carried along in the Stern layer is almost the same for LD and HD, which reveals that, in the LD case, the counterions are more densely packed in the Stern layer.

In order to investigate the mobility μ of the macroion as a function of its surface charge density $\sigma = Q/(4\pi R_{\text{M}}^2)$, two different types of simulations were performed. First, the charge Q was varied from $Q = 121 e$ to $801 e$ while keeping the radii R_{H} and R_{M} fixed at 10 \AA and 20 \AA , respectively. The number of counter- and coions used for a given value of Q are listed in Table I. Also included in this list is the Debye screening parameter $\kappa = [4\pi\lambda_{\text{B}}(N_{\text{ct}}+N_{\text{co}})/L^3]^{1/2}$ which was roughly kept constant around 0.13 \AA^{-1} . Secondly, runs for $Q = 255 e$ and $Q = 401 e$ were done in which the charge density σ was varied by choosing different macroion radii $10 \text{ \AA} \leq R_{\text{M}} \leq 20 \text{ \AA}$ in steps of 2 \AA or 2.5 \AA (note that the radius R_{H} remains fixed at 10 \AA in these runs). The results for the different runs are shown in Fig. 3 where μ is plotted as a

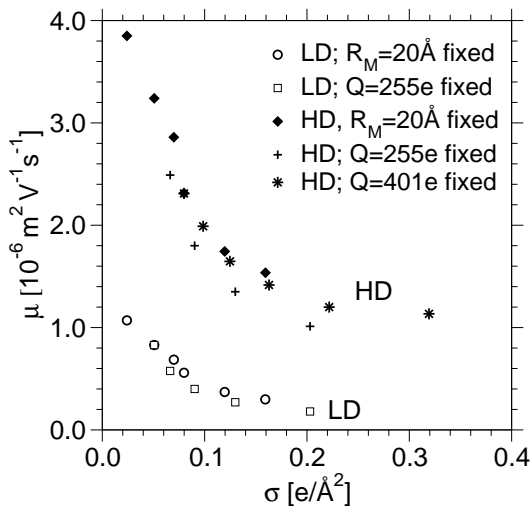


FIG. 3: The macroion mobility μ as a function of the surface charge density σ for LD and HD simulations as indicated. The charge density σ is either varied by changing the radius R_M of the macroion from 10 \AA to 20 \AA keeping Q fixed at $Q = 255 e$ or $Q = 401 e$, or by changing Q from $Q = 121 e$ to $Q = 801 e$ keeping R_M fixed at 20 \AA . The number of counterions and coions used for each value of Q is mentioned in text. For all data, the “hydrodynamic radius” is chosen to be constant at $R_H = 2.5 a = 10 \text{ \AA}$.

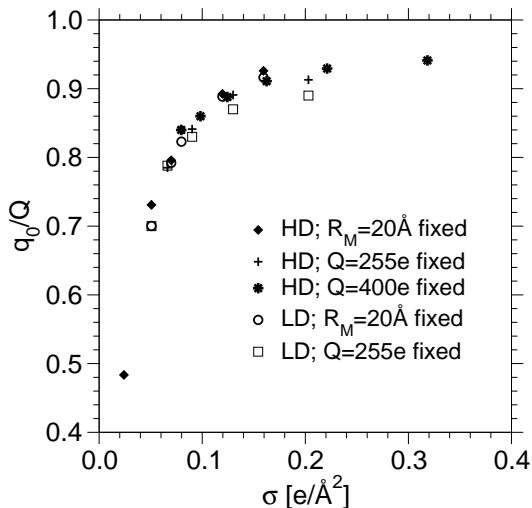


FIG. 4: Ratio q_0/Q as a function of σ . As indicated, in the different data sets either Q or R_M are fixed while σ is varied (see also Fig. 3).

function of σ for both HD and LD runs. In both cases, the mobility μ decreases with increasing σ . This behavior is in qualitative agreement with theoretical calculations for high values of the surface charge, i.e. $\sigma > 0.01 e/\text{\AA}^2$ (see Ref. [13] and references therein). Note that, at small σ the opposite behavior is observed, i.e. an increase of μ with σ [13].

For monovalent microions, Fig. 3 demonstrates that at

constant screening parameter κ the mobility μ is controlled by the surface charge density of the macroion. Discrepancies that can be seen in the plot might stem from the slight variation of κ in the different runs (see Table I). The LD runs that are shown in the figure exhibit a similar qualitative behavior. However, compared to HD, the LD data is shifted towards lower values of μ . This is because the hydrodynamic flow field is switched off in the LD simulations. The coupling of the LB fluid to the motion of the macroion leads to a backflow effect in the LB fluid which enhances the mobility of the macroion. This backflow effect yields also stronger correlations between the motion of the counterions and that of the macroion. Thus, as shown in Fig. 2, the reduced counterion velocity $V_{ct}(r)/V_M$ decays slower in the HD case than in the LD case.

The correlations between counterions and macroions are further considered in Fig. 4. Here, q_0/Q is plotted vs. σ . As before, we vary σ by changing R_M keeping Q fixed or by changing Q with R_M fixed at 20 \AA . As we see, the different data sets fall roughly onto one master curve (note that this is even true for the LD data). The functional behavior of q_0/Q reflects the one for μ . At small values of σ , the ratio q_0/Q is “rapidly” increasing (associated with a rapid decrease of μ) and it seems to saturate at high σ (as μ does). Thus, the electrophoretic mobility shows a saturation when q_0/Q is approaching unity. In the latter case, the electric field sees a “particle” with an effective charge $Q_{\text{eff}} = Q - q_0$.

The regime of low macroion charges Q has been studied recently by Lobaskin *et al.* [14] using a similar LB/MD

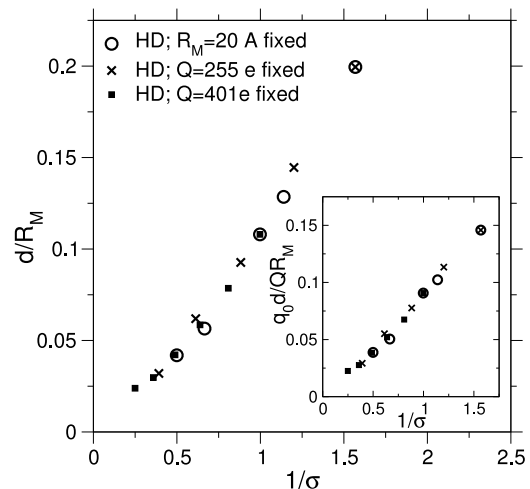


FIG. 5: Plot of the measure of distortion d of the Stern layer, normalised by the Coulomb radius of colloid R_M as a function of the inverse surface charge density $1/\sigma$ (for the definition of ‘ d ’ see text). The inset shows $q_0 d / QR_M$ which is a measure of the charge separation due to the distortion of the EDL.

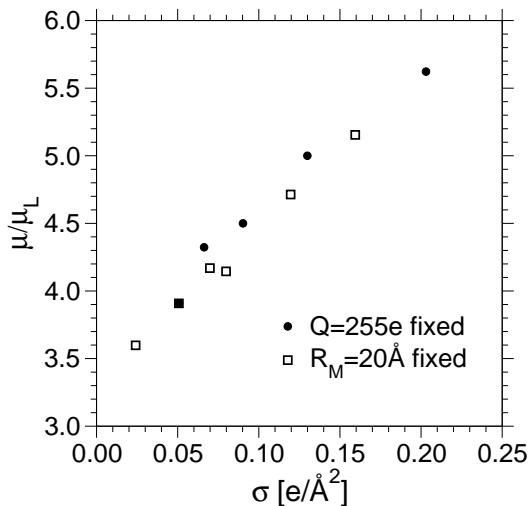


FIG. 6: Plot of $\mu_{\text{HD}}/\mu_{\text{LD}}$ versus the charge density σ . The mobilities μ_{HD} and μ_{LD} correspond to HD and LD runs, respectively.

technique. These authors considered a primitive model in the salt free regime (i.e. without coions). Their results agree with experimental data [15] for low Q , where an increase of μ with Q (σ) is observed. In this regime, μ is controlled by the bare charge Q as there is no significant dynamic Stern layer to create a shielding for Q . Hence the peak in μ observed in the experimental data of Martin-Molina *et al.* [13] denotes the point of crossover from this regime to a regime where μ is controlled by q_0/Q . For high values of σ , μ decreases with σ due to greater shielding for higher Q , whereas, for low values of σ (Q) the mobility increases with σ .

O'Brien and White [7] have proposed that the decrease in macroion mobility can be attributed to the increasing distortion of the EDL at high values of σ . To see whether the distortion of the charge cloud is indeed a relevant effect also at very high values of σ (considered in this work), we quantify the distortion of the EDL as follows: We compute the distance d of the center of mass (CM) of the EDL from the center of the macroion. Here, those counterions form the EDL which are within the *dynamic* Stern layer and move along the macroion. Figure 5 shows that the normalised distortion d/R_M and the normalised quantity q_0d/QR_M decrease with increasing σ . The quantity q_0d/QR_M is a measure of the charge separation between the center of the macroion and center of the counterion cloud. Thus, the amount of distortion becomes less pronounced with increasing σ . This rules out the mechanism proposed by O'Brien and White in the case of high values of σ .

We have already inferred from Fig. 2 that hydrodynamic backflow due to the LB fluid enhances the correlations between the counterion and the macroion motion as well as the absolute value of μ . In Fig. 6, the mobilities obtained from LD and HD runs (denoted by μ_{HD} and μ_{LD} , respectively) are directly compared to each other

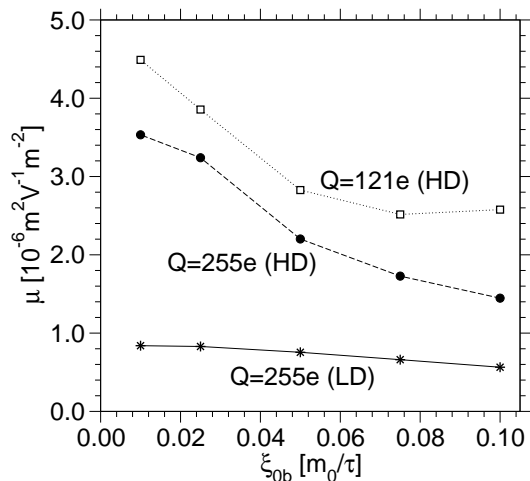


FIG. 7: Macroion mobility μ versus the counterion coupling constant ξ_{ob} for LD and HD simulations. The colloidal friction ξ_0 is fixed at $0.1m_0/\tau$ and $R_M = 20 \text{\AA}$. The lines are guides to the eye.

by plotting the ratio $\mu_{\text{HD}}/\mu_{\text{LD}}$ as a function of σ . We see that $\mu_{\text{HD}}/\mu_{\text{LD}}$ increases almost linearly with σ .

Microscopically, we understand this by noting that the higher macroion charge density leads to a higher number density of counterions per unit volume in the moving EDL of the colloid. The counterion coupling to the LB fluid results in an increased velocity of the LB fluid around the macroion at higher densities. Thus the macroion feels less frictional drag and, compared to the LD case, a higher value of μ is obtained.

In Fig. 7, it is further explored how the counterion coupling with the LB fluid affects the colloidal mobility. We keep the friction coefficient for the macroion coupling to the LB fluid, ξ_0 , fixed and vary that for the microion coupling, ξ_{ob} (for the definition see Sec. II). Whereas, for the HD simulations, μ decreases significantly with ξ_{ob} , in the LD case, μ exhibits only a weak dependence on ξ_{ob} . Thereby, the HD result tends to approach the one from LD for high values of ξ_{ob} . In the HD case, small values of ξ_{ob} mean a weaker coupling of the microion motion to that of the LB fluid, leading to an increase of the macroion mobility. The detailed understanding of this finding requires further investigation.

Note that, in the LD simulation for $Q = 121e$, a dynamic Stern layer cannot be formed, because the Coulomb attraction is too weak in this case. Hence, a high value of mobility results which is outside the range used in Fig. 7. On the other hand, in the HD simulation for $Q = 121e$ a well-defined dynamic Stern layer is seen and, as shown by Fig. 7, the behavior of μ is qualitatively similar to that at $Q = 255e$. This demonstrates the importance of the hydrodynamic flow field for the behavior of the electrophoretic mobility of weakly charged colloids.

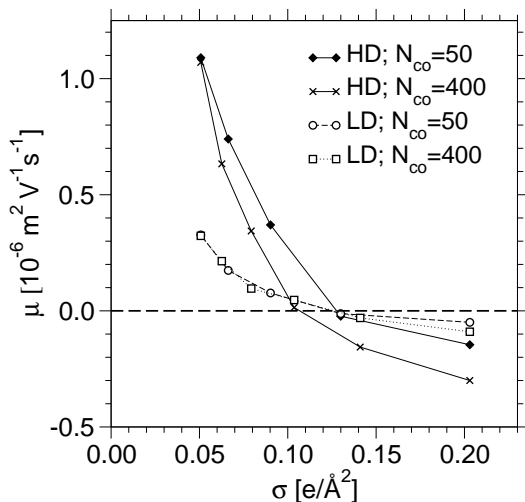


FIG. 8: Electrophoretic mobility μ as a function of surface charge density σ for two different systems using LD and HD, as indicated. The lines serve as guides to the eye.

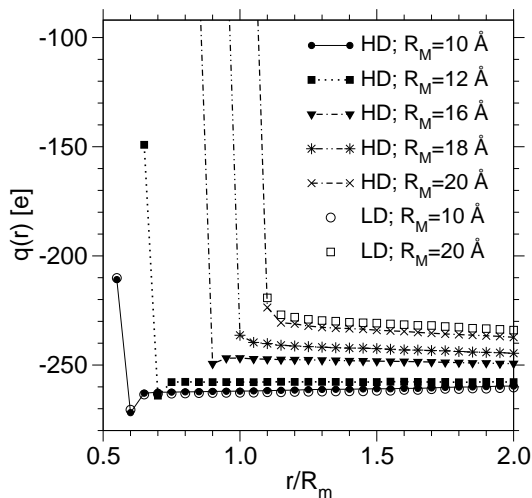


FIG. 9: Cumulative charge of divalent ions $q(r)$ as a function of r/R_m for different values of macroion radius R_M as indicated. Data for the system with $N_{ct} = 526$ divalent counterions and $N_{co} = 400$ divalent coions is shown (the charge of the macroion is $Q = 255e$). The distance r in the x-axis is normalised by $R_m = 20\text{\AA}$ which corresponds to the largest radius used.

B. Divalent salt ions

Charge inversion in the presence of multivalent counterions has been observed in static experiments and theoretical studies [12, 26, 36]. Experimentally charge inversion is detected using mainly electrophoresis. It is well established that charge inversion is due to counterion correlations and beyond the scope of mean-field theories. Our aim in this study is twofold: the onset charge density σ , at which charge inversion occurs, is determined and secondly, the extent of the Stern layer from HD sim-

ulations is compared to that from LD simulations.

To this end, two systems of a macroion of charge $Q = 255e$ mixed with divalent microions are considered, one with $N_{ct} = 526$ divalent counterions and $N_{co} = 400$ divalent coions, and the other one with $N_{ct} = 176$ divalent counterions and $N_{co} = 50$ divalent coions. In each case, 3 monovalent counterions are added to maintain charge neutrality. The charge density σ is varied by changing the radius of the macroion R_M from 10 to 20 \AA , thereby keeping the radius R_H fixed at 10 \AA . In Fig. 8, the mobility μ as function of σ is plotted for the different systems. Different from the case of monovalent microions, μ changes its sign in all cases, thus indicating that at high values of σ the macroion is moving opposite to the direction of the electric field. Overall, at a given value of σ , the mobility of the macroion in the presence of divalent microions is smaller than with monovalent ones.

Since the screening due to divalent microions is much more effective, the counterion charge density is higher near the colloidal surface than in electrolytes with monovalent microions. This can be seen in Fig. 9, where the cumulative charge $q(r)$ around the macroion is displayed for different values of R_M corresponding to different values of σ at the fixed macroion charge $Q = 255e$. We see that for $R_M \leq 16\text{\AA}$, $q(r)$ develops a local minimum near the colloidal surface. This indicates charge inversion (i.e. $|q(r)| > 255e$) and it explains the appearance of negative values of μ .

For comparison, we have plotted LD data in Fig. 9 for the largest and the smallest radii used, i.e., for $R_M = 20\text{\AA}$ and $R_M = 10\text{\AA}$, respectively. We see that the charge profile for LD and HD is nearly identical, which shows that the dynamic Stern layer is determined by the static Coulomb forces. For higher salt concentration, charge inversion is more pronounced, as seen by lower values of μ at high σ . Both LD and HD show the phenomenon of charge inversion at high values of σ . In particular in the HD case, charge inversion is more pronounced for higher salt concentration. As in the studies with monovalent counter- and coions, for divalent microions $|\mu_{LD}| < |\mu_{HD}|$ holds as well.

IV. CONCLUSIONS

In this work, a hybrid MD/LB scheme was used to investigate the electrophoretic mobility of a macroion in an electrolyte solution. We have considered highly-charged macroions ($\sigma = 38\text{ }\mu\text{C}/\text{cm}^2$ – $500\text{ }\mu\text{C}/\text{cm}^2$) for which theories based on the linearized electrokinetic equation are not applicable. For high values of the macroion's surface charge σ , experiments on systems with multivalent salt ions [13] have shown that the electrophoretic mobility μ can decrease with increasing σ for 2 : 1 salts whereas μ for 2 : 2 salts, it shows a plateau. In our simulations, we observe decrease of μ with σ for both 1 : 1 and 2 : 2 salt. Moreover, in contrast to previous theoretical studies [7],

we observe a lowering of μ with σ even for $\kappa R_M < 3$ for monovalent salt ions.

The authors of [13], attribute the lowering of μ in the 2 : 1 case to the presence of coions in the EDL. As we have demonstrated in this work, a decreasing μ as a function of σ requires the formation of a pronounced dynamic Stern layer of charge q_0 , consisting of counterions that move along the same direction as the macroion in the presence of an electric field. The lowering of μ is directly related to the increase of the quantity q_0/Q which we call the screening charge fraction. The absolute value of screening charge fraction $|q_0/Q|$ of the colloid-counterion cloud complex increases with increasing σ , reflecting a lowering of μ . Note that the number of coions in the dynamic Stern layer is negligible.

Furthermore, we observe charge inversion for divalent counter- and coions, but only when we reach sufficiently high values of σ . At very high values of σ , μ for colloidal systems with monovalent salt ions tends to saturate, because there is no space to add more counterions into the dynamic Stern layer. However, this is different when multivalent salt ions and counterions are used. Then, $|q_0/Q| > 1$ holds and μ becomes negative. The distribution of charge in the EDL for this case as a function of distance r from the center of the colloid is non-monotonic and completely different from what is expected from standard electrokinetic theories [5]. Though we have not carried out studies for the 2:1 salt case, it is possible that the discrepancy in the experimental results between the 2:1 and the 2:2 salt case arises from entropic/osmotic forces. The larger number of coions in the 2:1 salt (compared to the systems with a 2:2 salt) may lead to larger osmotic forces on the counterions which could result in larger values of q_0 for the 2:1 case. However, this issue can be resolved only after further investigations.

In the work of O'Brien and White [7], the lowering of

μ with the ζ potential has been attributed to the distortion of the EDL. Though the explicit measurement of the retarding force arising from the distortion of the EDL is outside the scope of this work, we have shown that the charge distortion within the dynamic Stern layer decreases with increasing σ . This is indicated by the lowering of the quantities d/R_M and $q_0 d/Q R_M$ with increasing σ . This observation combined with a host of other evidences presented in this paper, indicate that accumulation of charges in the Stern layer is the dominant mechanism for the lowering of μ as a function of σ , providing that high values of σ are considered.

By comparing the LB/MD (or HD) results to those from LD simulations, we were able to elucidate the role of hydrodynamic interactions. The structure of the Stern layer is more compact in the Langevin simulations. Hydrodynamic interactions enhance the electrophoretic mobility and so they have the opposite effect to electrostatic screening. This is due to a backflow effect in the fluid which pushes the counterions to move along the same direction as the macroion. Hydrodynamic forces have pronounced influence in the formation of the dynamic Stern layer, especially for low charges. An interesting finding is that the mobility as obtained from HD relative to that from LD exhibits an almost linear increase with σ . Further work on the role of hydrodynamic interactions for the electrophoresis of charged colloids is in progress.

Acknowledgment: We thank Burkhard Dünweg, Vladimir Lobaskin, and Thomas Palberg for stimulating discussions. We acknowledge financial support by the Deutsche Forschungsgemeinschaft (DFG) under Grants No. HO 2231/1 and HO 2231/2, by the SFB 625 "Von einzelnen Molekülen zu nanoskopisch strukturierten Materialien", and by the SFB TR6 "Colloidal Dispersions in External Fields". Generous grants of computing time on the JUMP at the NIC Jülich are gratefully acknowledged.

-
- [1] J. Lyklema, *Fundamentals of Colloid and Interface Science* (Academic, New York, 1995).
- [2] J. Lyklema and M. Minor, *Coll. Surf. A* **140**, 33 (1998).
- [3] R. J. Hunter, *Foundations of Colloid Science* (Oxford University Press, Oxford, 2001).
- [4] M. Lozada-Cassou, E. Gonzalez-Tovar, and W. Olivares, *Phys. Rev. E* **60**, R17 (1999).
- [5] W.B. Russel, D.A. Saville, and W.R. Schowalter, *Colloidal Dispersions* (Cambridge University Press, Cambridge, 1989).
- [6] P. H. Wiersema, A. L. Loeb, and J. T. G. Overbeek, *J. Coll. Int. Sci.* **22**, 78 (1966);
- [7] R. W. O'Brien and L.R. White, *J. Chem. Soc., Faraday Trans. 2* **74**, 1607 (1978).
- [8] H. Oshina, T.W. Healy and L.R. White, *J. Colloid Interface Sci.* **90**, 17 (1982).
- [9] F. Booth *Proc. Roy. Soc. A*, **203**, 514 (1950)
- [10] J. Th. T Overbeek, *Kolloidchem. Beihefte.*, **54**, 287 (1943).
- [11] B.V.R. Tata, *Curr. Sc.* **80**, 948 (2001).
- [12] K. Besteman, M.A.G. Zevenbergen, H.A. Heering, and S. G. Lemay, *Phys. Rev. Lett.* **93**, 170802 (2004).
- [13] A. Martin-Molina, M. Quesada-Perez, F. Galisto-Gonzalez, and R. Hidalgo-Alvarez, *J. Phys. Chem. B* **106**, 6881 (2002).
- [14] V. Lobaskin, B. Dünweg, and C. Holm, *J. Phys.: Condens. Matter*, **16** S4063 (2004).
- [15] V. Lobaskin, M. Medebach, Th. Palberg, B. Dünweg, and Ch. Holm, preprint cond-mat/0601588.
- [16] G.M. Torrie and J.P. Valleau, *J. Chem. Phys.* **73**, 5807 (1981).
- [17] R.R. Netz, *Phys. Rev. Lett.* **91**, 138101 (2003).
- [18] L. Joly, Ch. Ybert, E. Trizac, and L. Bocquet, *Phys. Rev. Lett.* **93**, 257805 (2004).
- [19] J. Horbach and S. Succi, *Phys. Rev. Lett.* **96**, 224503 (2006).
- [20] M. Patra, M. Patriarca and M. Kartunen, *Phys. Rev. E* **67**, 031402 (2003).
- [21] P. Wette, H.-J. Schöpe, and T. Palberg, *J. Chem. Phys.* **116**, 10981 (2002).

- [22] M. Medebach and T. Palberg, *J. Chem. Phys.* **119**, 3360 (2003).
- [23] M. Medebach and T. Palberg, *J. Phys.: Condens. Matter* **16**, 5653 (2004).
- [24] T. Palberg, M. Medebach, N. Garbow, M. Evers, A. Bareira Fontecha, and H. Reiber, *J. Phys.: Condens. Matter* **16**, S4039 (2004).
- [25] L. Shapran, M. Medebach, P. Wette, T. Palberg, H. J. Schöpe, J. Horbach, T. Kreer, A. Chatterji, *Coll. Surf. A* **270–271**, 220 (2005).
- [26] A. Yu. Grosberg, T.T. Nguyen, and B.I. Shklovskii, *Rev. Mod. Phys.* **74**, 329 (2002).
- [27] R. Benzi, S. Succi, and M. Vergassola, *Phys. Rep.* **222**, 145 (1992); S. Chen and G. Doolen, *Ann. Rev. Fluid Mech.* **130**, 329 (1998); S. Succi, *The Lattice Boltzmann equation* (Oxford Univ. Press, Oxford, 2001).
- [28] K. Kim, Y. Nakayama, and R. Yamamoto, *Phys. Rev. Lett.* **96**, 239902 (2006).
- [29] A. Chatterji, J. Horbach, *J. Chem. Phys.* **122**, 184903 (2005).
- [30] A. Chatterji and J. Horbach, *Mathematic and Computers in Simulation.*, accepted for publication (2006).
- [31] T. Kreer, J. Horbach, A. Chatterji, *Nonlinear effects in charge stabilized colloidal suspensions*, *Phys. Rev. E*, accepted for publication (2006); preprint cond-mat/0602250.
- [32] M.P. Allen and D.J. Tildesley, *Computer Simulation of Liquids* (Clarendon Press, Oxford, 1987).
- [33] D. Frenkel and B. Smit, *Understanding Molecular Simulation: From Algorithms to Applications*, 2nd edn (Academic Press, San Diego, 2002).
- [34] A.J.C Ladd, *J. Fluid Mech.* **271**, 285 (1994); *J. Fluid Mech.* **271**, 311 (1994).
- [35] P. Ahlrichs and B. Dünweg, *J. Chem. Phys.* **111**, 8225 (1999).
- [36] R. Messina, C. Holm, and K. Kremer, *Phys. Rev. Lett.* **85**, 872 (2000); R. Messina, C. Holm, and K. Kremer, *Europhys. Lett.* **51**, 461 (2000).